Weakening Trend in the Atmospheric Heat Source over the Tibetan Plateau during Recent Decades. Part II: Connection with Climate Warming

ANMIN DUAN AND GUOXIONG WU

State Key Laboratory of Numerical Modelling for Atmospheric Sciences and Geophysical Fluid Dynamics, Institute of Atmospheric Physics, Chinese Academy of Sciences, Beijing, China

(Manuscript received 30 June 2008, in final form 2 March 2009)

ABSTRACT

In Part I the authors have shown that heating sources in spring over the Tibetan Plateau (TP), and in particular the sensible heat flux (SHF), exhibit a significant weakening trend since the mid-1980s that is induced mainly by decreased surface wind speed. The possible reason of such a change is further investigated in Part II by analyzing historical observations and the NCEP/Department of Energy (DOE) reanalysis. The steady declining trend in the surface wind speed over the TP after the 1970s arises mainly from the zonal component. Since the mean altitude of the TP is about 600 hPa and the surface flow is controlled by the East Asian subtropical westerly jet (EASWJ) for most parts of the year, the substantial tropospheric warming in the mid- and high latitudes to the north of the plateau results in a decrease of the meridional pressure gradient in the subtropics. As a result, the EASWJ and the surface winds over the TP are decelerated. Moreover, changes of the general circulation in the twentieth century simulated by 16 coupled climate models driven by natural and anthropogenic forcings are examined. Intercomparison results suggest that sulfate aerosol indirect effects and ozone may be important in reproducing the weakening trend in EASWJ. Although nearly half of the models can successfully reproduce the observed trends in the EASWJ during the last two decades, there is an obvious spread in simulation of the spatial patterns of twentieth-century tropospheric temperatures, suggesting significant room still exists for improvement of the current state-of-the-art coupled climate models.

1. Introduction

Because of its significant mechanical and thermal forcings, the Tibetan Plateau (TP) exerts great influences upon the neighboring circulation pattern and the downstream weather and climate anomalies (e.g., Yin 1949; Yeh and Zhu 1955; Flohn 1957; Hahn and Manabe 1975; Yeh and Gao 1979; Yanai et al. 1992). On the interannual time scale, for example, a clear positive correlation exists between the spring heating source over the TP and the subsequent summer monsoon precipitation in the valleys of the Yangtze River and Huaihe River, whereas a negative correlation is obvious between the spring TP heating and the summer rainfall in north China (Zhao and Chen 2001; Duan et al. 2005). Besides the thermal forcing of the TP, activities of cold air in the mid- and higher latitudes, variations of the subtropical high over the western Pacific, the ENSO cycle, and the land–air interaction also modulate the interannual variability of the East Asian summer monsoon (EASM) to a different degree (e.g., Tao and Chen 1987). Based on meteorological station observations and satellite data, in Part I of this study (Duan and Wu 2008, hereafter Part I) we found that the strength of the spring heat source over the TP, which depends largely on the component of sensible heat flux (SHF), has experienced a significantly weakening trend during the period of 1980–2003. The steady decline of surface wind speed contributes largely to such a change in SHF.

However, recent observational evidence indicates that EASM precipitation in the valleys of the Yangtze River and Huaihe River increased substantially after the 1970s, accompanied by aggravated drought in North China and floods in South China (Hu et al. 2003; Ding and Sun 2004). An inconsistency thereby exists between the interannual and interdecadal variations in spring TP thermal forcing and the EASM. In addition, the steady

Corresponding author address: Anmin Duan, LASG, Institute of Atmospheric Physics, Chinese Academy of Sciences, P.O. Box 9804, Beijing 100029, China.
E-mail: amduan@lasg.iap.ac.cn

DOI: 10.1175/2009JCLI2699.1

declining trend in wind speed is a widespread phenomenon over East Asia (EA), not only on the surface (Xu et al. 2006), but also in the mid- and lower troposphere (Duan 2007). All these facts imply that there might be a change in large-scale circulation responsible for the weakening trend in both the spring TP heating source and the EASM.

Some analyses and modeling results suggest that the interdecadal variability of the general circulation in the Northern Hemisphere is a result of the interdecadal variability of sea surface temperatures (SST) over the central and eastern tropical Pacific, and that the impact is realized mainly through the Pacific–North American (PNA)-like pattern (e.g., Nitta and Yamada 1989; Trenberth and Hurrell 1994). Hu (1997) argues that the interdecadal variability of summer rainfall and temperatures over EA is largely influenced by the change of SST and convective activity in the tropical Indian Ocean and tropical western Pacific through intensifying the Hadley cell and the subtropical high. In reality, the climate variability in EA is extremely complicated because of the complex interlacing of land–sea surfaces in the geographic location, gigantic topographic effects, and the variety of underlying surfaces. Besides the signals originating from the tropics, substantial climate warming in the mid- and high latitudes over eastern Eurasia is another likely factor in determining the trend in the EASM system. Recently, Xu et al. (2006) explored this possibility and emphasized the local impacts from human activities such as air pollution.

The main objectives of this paper, therefore, are to clarify the connection between the change in surface wind speed over the TP and the large-scale circulation shift through data diagnosis and multimodel intercomparison. The organization of this text is as follows. Section 2 gives a brief description of data and models. Section 3 investigates the association of the change of the East Asian subtropical westerly jet (EASWJ) with the trend in heating sources over the TP. In section 4, 16 climate models results are evaluated to illustrate the impacts of global warming on the general circulation shift. Section 5 summarizes the major results and provides some discussion.

2. Data and models

a. Data

Six-hourly wind direction at 10 m above the surface of 71 regular surface meteorological observation stations in the central and eastern TP (CE-TP) and 3 in the western TP (W-TP) are provided by China Meteorological Administration (CMA; detailed information about this dataset is explained in section 2 of Part I). As introduced in Part I, to ensure a reliable outcome, the temporal evolution of data from 37 stations in the period of 1961–2003 and 71 stations in 1980–2003 are compared simultaneously in the CE-TP. The 26-yr (1979–2004) monthly mean air temperature, geopotential height, zonal and meridional wind speed, and vertical velocity fields in the National Centers for Environmental Prediction/Department of Energy (NCEP/DOE) reanalysis 2 (Kanamitsu et al. 2002; for details see http://www.cpc.ncep.noaa.gov/products/wesley/reanalysis2/kana/reanl2-1.htm) are adopted to investigate the large-scale circulation variation. The horizontal resolution is 2.5° × 2.5° for these variables at 17 standard pressure levels, and 500 hPa is chosen to represent the lower free atmosphere over the TP. Despite some intrinsic limitations of the quality of reanalysis, especially for surface variables, it is acceptable to investigate the evolution and pattern for large-scale circulation in the upper atmosphere. For example, using the NCEP–National Center for Atmospheric Research (NCAR) reanalysis, Yu et al. (2004) found a distinctive strong tropospheric cooling trend (1980–2001 minus 1958–79) in EA during July and August at 200 hPa, accompanying the southward shift of the upper-level westerly jet stream over EA. By comparing three meteorological reanalysis [NCEP–NCAR, NCEP/DOE, and the 40-yr European Centre for Medium-Range Weather Forecasts (ECMWF) Re-Analysis (ERA-40; Uppala et al. 2005)] with three outgoing longwave radiation (OLR) datasets, Hu and Fu (2007) showed that the Hadley circulation has had a significant expansion of about 2° to 4.5° latitude in summer and fall since 1979. Over the TP, the observed warming trend in the midtroposphere and a cooling trend in the lower stratosphere can be identified from ERA-40 to a considerable degree (Duan et al. 2006).

b. Model

The 16 coupled atmosphere–ocean general circulation models (AOGCMS) employed in this study are based on the contributions to the Coupled Model Intercomparison Project (CMIP) for the Intergovernmental Panel on Climate Change (IPCC) Fourth Assessment Report (AR4). General information, together with the natural and anthropogenic forcings used by the different modeling groups (for details about these models see http://www-pcmdi.llnl.gov/ipcc/about_ipcc.php) is listed in Table 1. The horizontal resolution varies from 4° × 5° (GISS-ER) to 1.406 25° × ~1.406 25° (CCSM3.0). The simulation scenario is the twentieth-century climate in coupled models (20C3M), in which the forcings are the combinations of greenhouse gases, sulfate aerosols, ozone, volcanic aerosols, and solar variability based on the historical data. Well-mixed greenhouse gases (GHGs)

TABLE 1. Name, institution and model expansion, resolution, and forcings used in IPCC simulations of twentieth-century climate. SO: solar irradiance; VL: volcanic aerosols; SD: sulfate aerosol direct effects; SI: sulfate aerosol indirect effects; GHG: well-mixed greenhouse gases; O: tropospheric and stratospheric ozone; LU: land use change; BC: black carbon; OC: organic carbon; MD: mineral dust; and SS: sea salt. A letter "Y" denotes inclusion of a specific time-varying forcing, with changes on interannual and longer time scales. Forcings that were varied over the seasonal cycle only, or not at all, are identified with a dash. A question mark indicates a case where there is uncertainty regarding inclusion of the forcing.

Model	Center and model expansion	Resolution	SO	VL	SD	SI	GHG	O	LU	BC	OC	MD	SS
BCCR-BCM2.0	Bjerknes Centre for Climate Research Bergen Climate Model version 2.0	T63	—	—	Y	—	Y	—	—	—	—	—	—
CCSM3.0	NCAR Community Climate System Model, version 3	T85	Y	Y	Y	—	Y	Y	—	Y	—	—	—
CGCM3.1(T47)	Canadian Centre for Climate Modelling and Analysis (CCCma) Coupled General Circulation Model version 3.1	T47	—	—	Y	—	Y	Y	—	—	—	—	—
CNRM-CM3	Centre National de Recherches Météorologiques Coupled Global Climate Model, version 3	T42	—	—	Y	Y	Y	Y	—	—	?	Y	Y
CSIRO Mk3.0	Commonwealth Scientific and Industrial Research Organisation Mark version 3.0	T63	—	—	Y	—	Y	—	—	?	?	?	—
GFDL CM2.1	Geophysical Fluid Dynamics Laboratory Climate Model version 2.01	2.5° × 2.0°	Y	Y	Y	—	Y	Y	—	Y	Y	—	—
GISS-AOM	Goddard Institute for Space Studies Atmosphere–Ocean Model	4° × 3°	—	—	Y	—	Y	—	—	—	—	—	Y
GISS-ER	GISS Model E-R	4° × 5°	Y	Y	Y	Y	Y	Y	—	Y	Y	Y	Y
FGOALS-g1.0	State Key Laboratory of Numerical Modeling for Atmospheric Sciences and Geophysical Fluid Dynamics (LASG)/Institute of Atmospheric Physics Flexible Global Ocean–Atmosphere–Land System Model gridpoint version 1.0	2.8° × 2.8°	Y	—	Y	—	Y	—	—	—	—	—	—
INM-CM3.0	Institute of Numerical Mathematics Coupled Model, version 3.0	5° × 4°	Y	Y	Y	Y	Y	—	—	—	—	—	—
IPSL CM4	L'Institut Pierre-Simon Laplace Coupled Model, version 4	2.5° × 3.75°	—	—	Y	Y	Y	—	—	—	—	—	—
MIROC3.2(medres)	Center for Climate System Research (CCSR)/National Institute for Environmental Studies (NIES)/Japan Agency for Marine-Earth Science and Technology (JAMSTEC) Model for Interdisciplinary Research on Climate 3.2, medium-resolution version	T42	Y	Y	Y	Y	Y	Y	Y	Y	Y	Y	Y

TABLE 1. (*Continued*)

Model	Center and model expansion	Resolution	SO	VL	SD	SI	GHG	O	LU	BC	OC	MD	SS
MPI ECHAM5	Max Plank Institute for Meteorology (MPI) ECHAM5	T63	—	—	Y	Y	Y	Y	—	—	—	—	—
MRI CGCM2.3.2	Meteorological Research Institute Coupled General Circulation Model version 2.3.2	T42	Y	Y	Y	—	Y	—	—	—	—	—	—
UKMO HadCM3	Third climate configuration of the Met Office (UKMO) Unified Model	1.25° × 1.875°	—	—	Y	Y	Y	Y	—	—	—	—	—
UKMO HadGEM1	UKMO Hadley Centre Global Environmental Model version 1	1.25° × 1.875°	Y	Y	Y	Y	Y	Y	Y	Y	Y	—	—

and the direct effects of sulfate aerosol are included simultaneously in all 16 models, whereas indirect effects of sulfate aerosol and tropospheric and stratospheric ozone effects are included only in 6 of them [i.e., CNRM-CM3.0, GISS-ER, MIROC3.2 (medres), MPI ECHAM5, UKMO HadCM3, and UKMO HadGEM1]. Since most of the simulation results for the 20C3M scenario end in 1999 or 2000 and the steady declining trend in the surface wind speed over the TP happens after the 1970s, the simulation results during the period of 1979–2000 are compared with each other. Previous studies have demonstrated that four models (CNRM-CM3, GFDL CM2.1, GISS-AOM, and MRI CGCM2.3.2) have good correlations of exceeding 0.40 from 1880 to 1999 with the observed surface air temperature averaged over China (Zhou and Yu 2006), and GFDL CM2.1 and MIROC3.2(medres) have good performance in reproducing the surface and upper-atmospheric temperature trends over the TP and China (Duan et al. 2006; Duan 2007).

As in Part I, linear variation rate (LVR) is used to depict the trend in meteorological variables, and the 95% confidence level is defined as the threshold of significant change.

3. Mechanism of the weakening trend in the SHF

a. Connection between surface wind over the TP and the EASWJ

The TP is located in the subtropics, and meteorological stations are usually established on plains or in the valleys of the east–west-oriented mountains, and thus the near-surface wind direction is typically westerly or southwesterly. Figure 1 presents the distribution of the seasonal mean wind direction during the period of 1979–2003. One can see that, from spring [March–May (MAM)] to winter [December–February (DJF)], the prevailing wind direction turns clockwise from south-southwesterly (SSW) to west-southwesterly (WSW) in the western and northern CE-TP, and from WSW to westerly (W) in the southeastern CE-TP, with gradually increasing strength of the zonal component. After the summer monsoon onset in late spring or summer [June–August (JJA)], an obvious southerly component prevails over the CE-TP.

Figure 2 shows the seasonal mean temporal evolution of surface wind direction over the CE-TP. Generally, there has been no significant change in the spring surface wind direction during the entirety of the last four decades. However, after the late 1980s, there is an increasing trend in the westerly component during spring and summer (JJA), and an increasing trend in

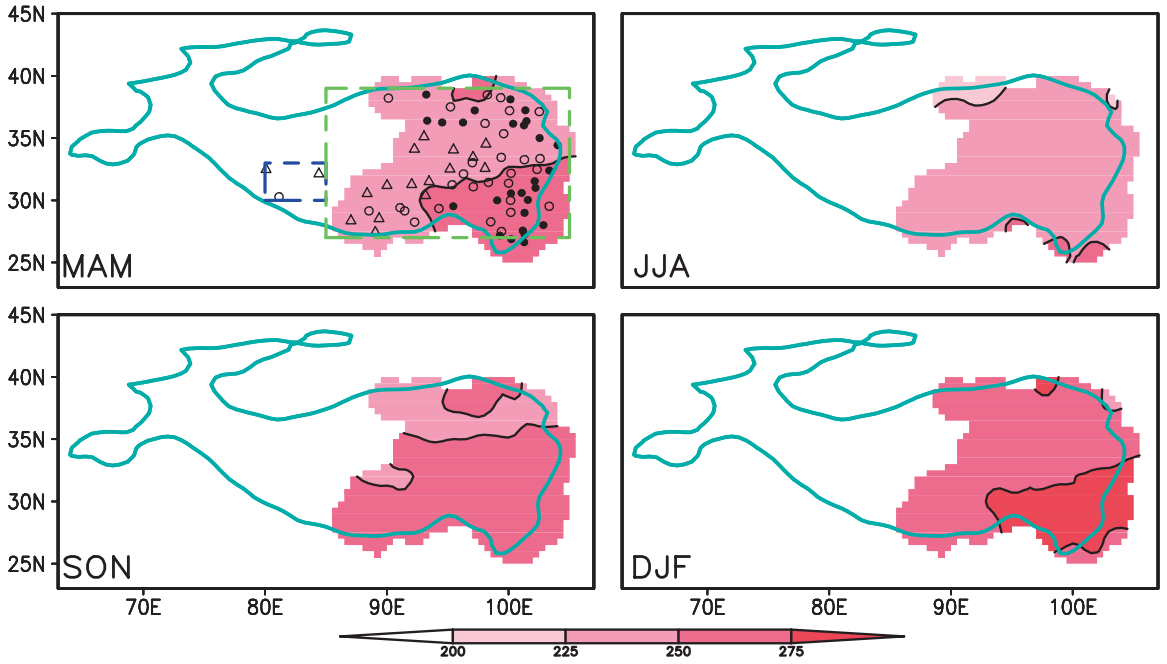

FIG. 1. Seasonal mean surface wind direction during 1979–2003 represented in units of degrees (0°, 90°, 180°, and 270° represent winds blowing from north, east, south, and west, respectively). Triangles, open circles, and solid circles denote stations above 4000, 3000, and 2000 m MSL. The thick curve outlines the TP area with an averaged altitude higher than 2500 m MSL. Two dashed boxes in the top left panel denote the (left) W-TP and (right) CE-TP areas.

the northerly component during autumn [September–November (SON)] and winter. The seasonal mean surface wind direction averaged over three stations in W-TP (Fig. 3) is very similar to that in the CE-TP, with an obvious southwesterly in JJA and strong westerlies in DJF. However, compared to the 1980s, the wind direction in the 1990s exhibits a larger seasonal variation, with a remarkably intensified southerly (northerly) component in JJA (DJF).

As revealed in Part I, the weakening trend in the wind speed over the TP occurs in the whole mid- and lower troposphere throughout most parts of the year. Naturally, people would like to connect this change to the shift in the large-scale circulation. In the upper troposphere and lower stratosphere, a narrow but strong westerly belt with large horizontal and vertical wind shears exists over subtropical East Asia, and it is known as the EASWJ. The EASWJ exhibits robust seasonal

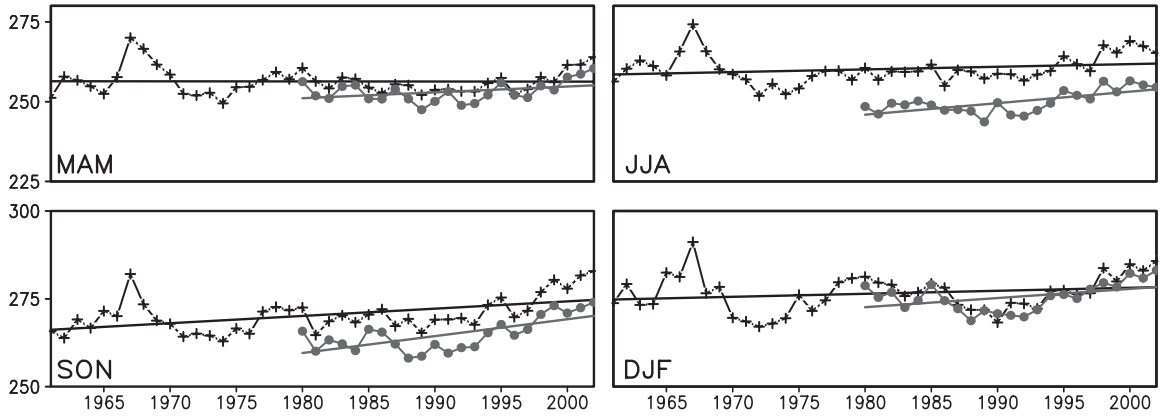

FIG. 2. Temporal evolution of seasonal mean surface wind direction during 1961–2003 (37-station average, crosses) and 1979–2003 (71-station average, circles) over the CE-TP. Solid lines denote their LVR.

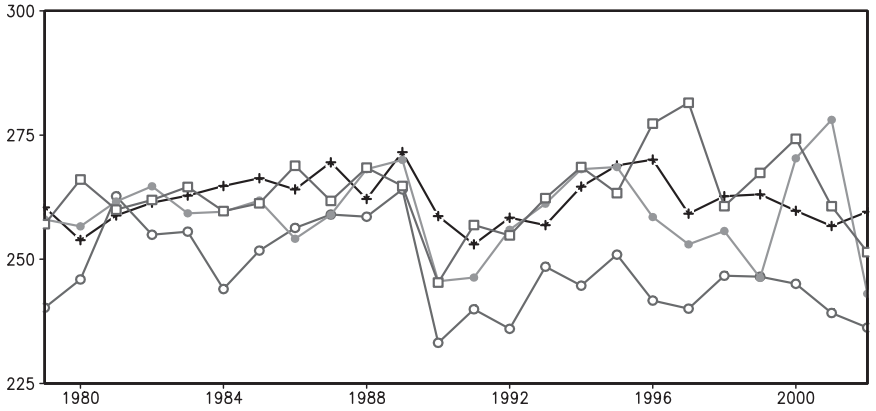

FIG. 3. Temporal evolution of seasonal mean surface wind direction over the W-TP during 1979–2003 (3-station average). Curves with crosses, open circles, solid circles, and open squares are for MAM, JJA, SON, and DJF, respectively.

evolutions in both intensity and location and is closely linked to the monsoon climate in EA (Yin 1949; Yeh and Zhu 1955; Zhang et al. 2006). The tropospheric air current over the TP is controlled by the strong EASWJ except in summer, when the EASWJ weakens substantially and moves poleward to the north of the TP (Fig. 4). The huge topography poses an obstacle for the westerly jet and splits it into two branches to the north and south borders of the plateau, resulting in a relatively weak wind region of typically less than 10 m s^{-1} at 500 hPa over the TP domain. On the other hand, the existence of the TP helps to maintain the core of the jet over the North Pacific downstream of the TP. The strongest EASWJ appears in winter (~16 m s^{-1}) and spring (~12 m s^{-1} at 500 hPa). In summer, however, owing to the activity of the EASM and the substantially strengthened poleward wind component, the EASWJ reduces to about 5 m s^{-1}. Note that 500 hPa represents the midtroposphere to the north and south sides of the plateau but is just above the lower boundary within the TP domain. According to the geostrophic balance relationship, the intensity of near-surface wind over the TP actually relies on the pressure gradient to its north and south sides. In the vertical direction, the core of the EASWJ inclines poleward slightly, with a maximum near 200 hPa (figure not shown).

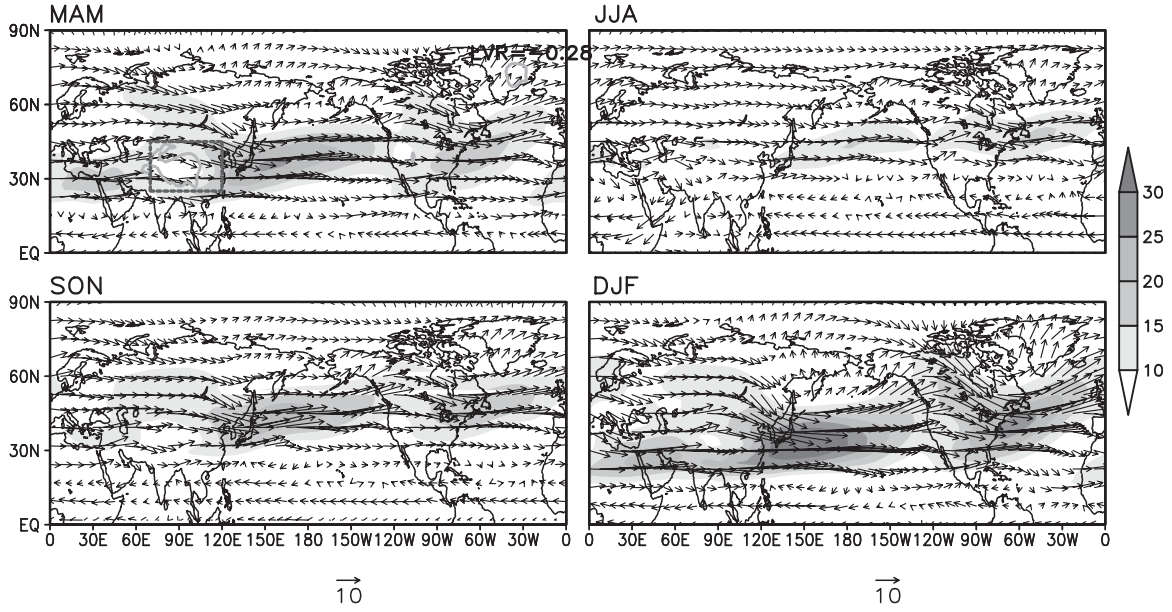

FIG. 4. Seasonal mean 500-hPa wind vector and wind speed during 1979–2003. The units of wind speed are m s^{-1}. The solid thick curves and dashed box in the top left panel denote the TP area EASWJ domain (25°–45°N, 70°–120°E), with height above 2500 m MSL.

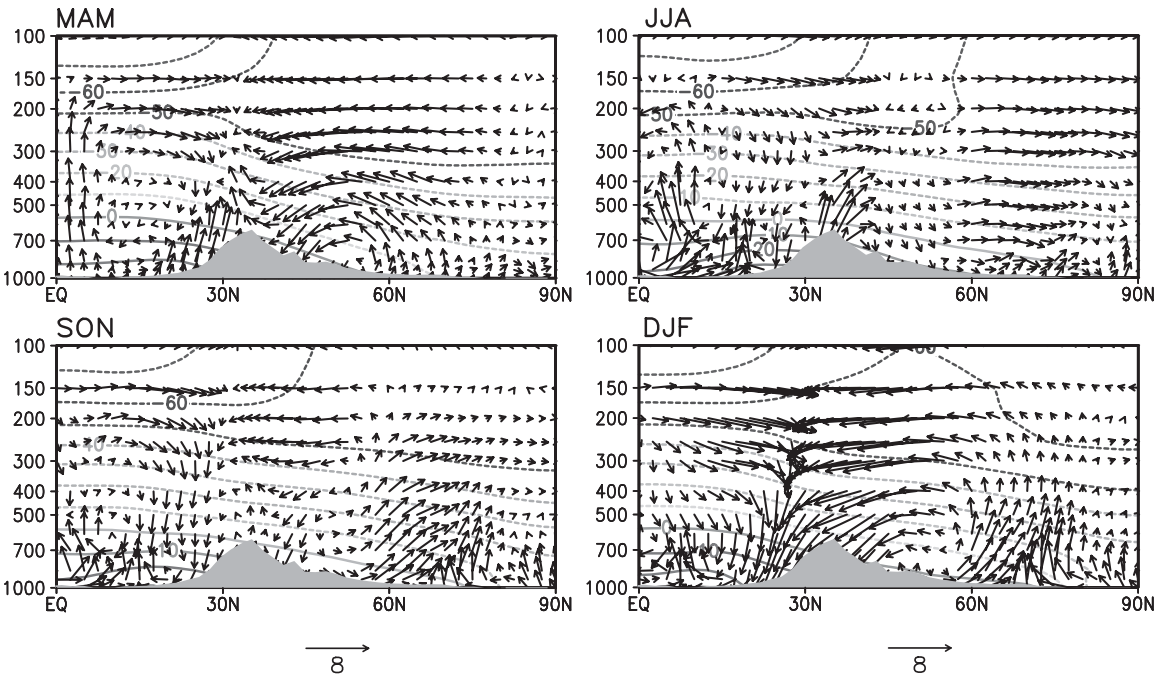

FIG. 5. Cross section of air temperature and meridional circulation averaged from 70° to 120°E during 1979–2003. The units of temperature, meridional wind speed (v), and vertical velocity (ω) are °C, m s^{-1}, and Pa s^{-1}, respectively. The meridional circulation is represented by the vector constructed by (v, $\omega \times -100$). Shaded areas denote topography.

Figure 5 presents the seasonal mean cross section of air temperature and meridional cell along 70°–120°E. Typically the poleward tropospheric temperature gradient leads to zonal westerlies over the subtropics, as well as mid- and high latitudes, as seen before. In the tropics, the poleward isotherms are flat with the warm center usually located to the south side of the huge orography (roughly at 20°N). As a part of the global circulation system, the mean easterly and westerly belts are closely connected with the meridional circulation in the vertical. Corresponding to the seasonal evolution of the EASWJ, the strongest and weakest Hadley cell circulations appear in winter and summer, respectively. In winter, the ascending branch moves southward to the Southern Hemisphere and the descending branch dominates the tropical and subtropical regions. In summer, the diminished meridional temperature gradient, together with the EASM precipitation accompanying ascending motion, impairs substantially the local Hadley cell. Spring and autumn are the so-called transition seasons between summer and winter, and the intensity and extent of the Hadley cell is medium. As discussed by many authors (e.g., Yeh and Gao 1979; Yanai et al. 1992), owing to strong heating during the summer half of the year, the vigorous ascending motion over the TP is accompanied by a reversed monsoon cell with compensating descending motion to both sides. This tends to reduce the local Hadley cell and Ferrel cell in MAM and JJA.

b. Trends in EASWJ

To conveniently investigate the change in the EASWJ, we define an index by calculating the average of the 500-hPa zonal wind speed within the EA domain (dashed box in the top left panel of Fig. 4) because 500 hPa generally represents the lower free atmosphere above the TP. The temporal evolution and the corresponding LVR of the EASWJ index are exhibited in Fig. 6. It shows an overall decreasing trend during the period of 1979–2003 in all seasons, and the significance of the trend is above the 95% confidence level in JJA (-0.54 m s^{-1} decade^{-1}), MAM (-0.31 m s^{-1} decade^{-1}), and SON (-0.24 m s^{-1} decade^{-1}). In winter, the LVR of the EASWJ is -0.23 m s^{-1} decade^{-1}. Compared to the significant decreasing trend in the zonal wind, the change of the 500-hPa meridional wind in the same domain is negligible (figure not shown). Therefore, the weakening trend in the surface and tropospheric wind over the TP and EA occurs primarily in the zonal component.

The geostrophic balance relationship suggests that such a large-scale change in zonal wind speed should be induced by the reduction of the in situ meridional pressure gradient. To clarify this point, in Fig. 7 we show

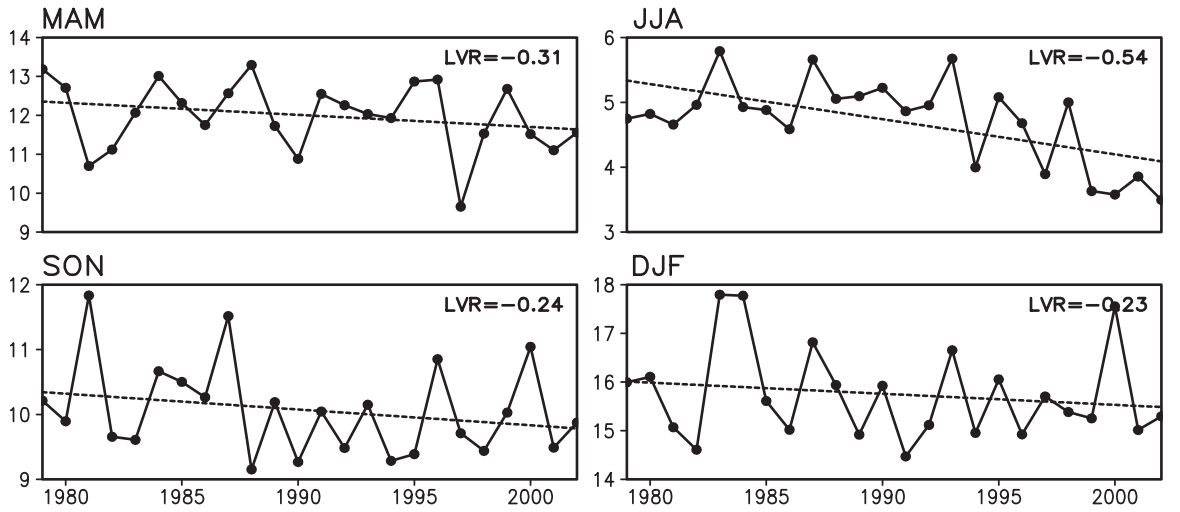

FIG. 6. Temporal evolution (solid curves) and LVR (dashed lines) of 500-hPa EASWJ index during 1979–2003. Units for EASWJ and its LVR are m s^{-1} and m s^{-1} $decade^{-1}$, respectively.

the spatial distribution of LVR in air temperatures, geopotential heights, and zonal wind speed at 500 hPa. From spring to summer, a warming trend of more than 0.4°C $decade^{-1}$ exists over Baikal and Mongolia, and the warming center moves southeastward to north China, Japan, and the North Pacific in autumn and winter. Moreover, another warming center with comparable LVR can be seen from the Kamchatka Peninsula to Alaska in spring. Northwest from the Siberian and Mongolian warming center, a cooling center (−0.4°C $decade^{-1}$) exists from summer to winter. Noteworthy is that the signal in temperature changes is much weaker in tropical Asia. Solomon et al. (2007) have also reported a generally larger warming amplitude over the midlatitudes than the tropics for both the surface and the troposphere during 1979–2005. To the east of the TP, there is a summer cooling center with LVR of −0.2°C $decade^{-1}$ over central and southern China, which has been documented by Yu et al. (2004) and linked with stratospheric cooling and the interaction

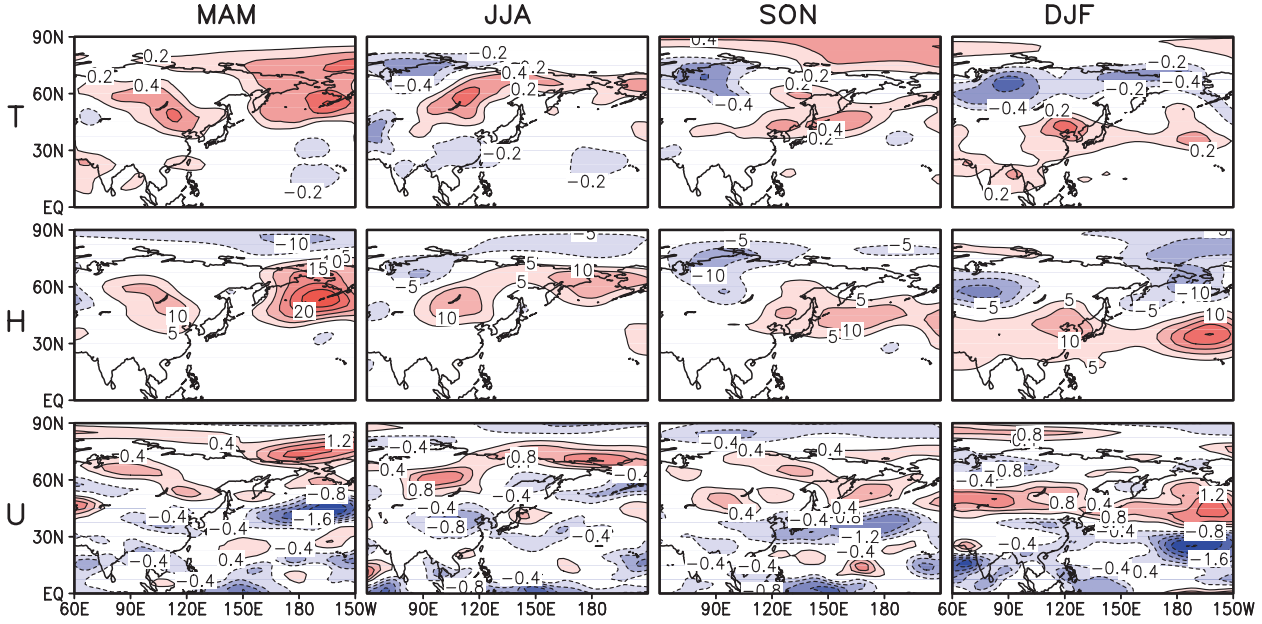

FIG. 7. Spatial distribution of LVR for (top) air temperature (°C $decade^{-1}$), (middle) geopotential height (gpm $decade^{-1}$), and (bottom) zonal wind speed (m s^{-1} $decade^{-1}$) at 500 hPa during 1979–2003. From left to right are MAM, JJA, SON, and DJF.

between the stratosphere and troposphere. As a result of temperature changes, geopotential height rises in warming areas and drops in cooling areas. Such a change in geopotential heights over the Asian continent (5–10 gpm decade^{-1}) enhances the climate mean Mongolian ridge in spring and summer and weakens the EA trough in autumn and winter. It further leads to a diminished meridional pressure gradient and a subsequently weakened zonal geostrophic wind to the south of the warming center. Similar to temperature and geopotential height, the change of the zonal wind speed is also seasonally dependent. A continental center with decreasing speeds of -0.2 m s^{-1} decade^{-1} appears in the region of 30°–45°N, 80°–120°E during spring and summer. In autumn and winter, it merges with another center over the North Pacific at the same latitudes. The EASWJ, therefore, has exhibited a pronounced declining trend during the last two decades, which can be attributed to the decreased meridional temperature and pressure gradients. The declining trend in the subtropical westerly jet is accompanied by an intensifying trend in the zonal wind over mid- and high latitudes. Also, regional features of climate change are evident. Two centers of LVR in the 500-hPa EASWJ can be seen over eastern China (-0.8 m s^{-1} decade^{-1}) and the mid-Pacific (-2.0 m s^{-1} decade^{-1}), with a remarkable equatorward shift from summer to winter.

Based on the principle of thermal wind, the variation of zonal wind with altitude depends on the meridional gradient of air temperatures. If air temperatures are decreased poleward, the westerlies increase or the easterlies decrease with altitude. The decreasing trend in the poleward temperature gradient at 500 hPa should be accompanied by a large declining trend in the westerlies in the upper troposphere over the TP, and this is true as shown in Fig. 11 of Part I, in which one can see a center of decreasing wind, as measured by 12 nearby radiosonde stations near 250 hPa in March and April during 1980–2003.

The increasing trend of surface temperatures induces a trend of enhanced convective activity over the tropical Indian Ocean and tropical western Pacific (Nitta and Yamada 1989). As a result, the Hadley cell is intensified and it further leads to a positive anomaly and southwest extension of the subtropical high. Hu (1997) and Gong and Hu (2002) indicated that heating in the Indian Ocean may play a key role in the interdecadal variation of the summer climate in China via such a circulation shift. The trend for temperature profiles and local meridional circulations, in terms of the constructed vector from LVRs of meridional wind speed and vertical motion during the period of 1979–2003, is presented in Fig. 8. The most significant change in the tropospheric air temperature is the striking warming center near the North Pole (1°C decade^{-1}). Over the tropics and midlatitudes, a 0.2°–0.4°C decade^{-1} warming trend occurs in the mid- and lower troposphere, with larger amplitudes appearing to the north of the seasonal mean EASWJ. Above it, a clear cooling trend exists in the upper troposphere and lower stratosphere. On the other hand, the change in the local meridional circulation over EA features a coherent weakening trend in the Ferrel cell throughout the year, with anomalous upward (downward) motion near 40°N (60°N). A similar result has been reported by Hu et al. (2005) and Hu and Fu (2007) in two other widely used reanalysis datasets, that is, NCEP–NCAR reanalysis (Kalnay et al. 1996) and ERA-40. On the other hand, the trend in the local Hadley cell is somewhat more complicated, with an intensifying trend in DJF. In JJA the monsoon cell, which is related to the Hadley cell, presents a clear strengthening trend. In fact, excessive monsoon rainfall in the valleys of the Yangtze River and Huaihe River after the 1970s has been considered as a symbol of recent climate change in China (Hu et al. 2003; Ding and Sun 2004). In MAM and SON, the equatorward ascending branch features a weakening trend, but the descending branch around 30°N shows an opposing intensifying trend, leading to a blurry signal for the trend of the local Hadley cell.

According to the dynamics of the general circulation (Holton 1992), a decrease in the meridional temperature gradient will induce a trend in the atmospheric baroclinicity and the regional Eliassen–Palm (E–P) flux divergence. Because the Ferrel cell is driven by eddy activity, such a change should be responsible for a weakening trend in the Ferrel cell. Recently Hu and Fu (2007) found the trend in the global Hadley cell has been characterized by poleward expansion and broadening of the cell in summer and fall since 1979. Possible mechanisms include the enhanced greenhouse effect induced weakening of baroclinic wave activity (Lu et al. 2007), ozone depletion (Polvani and Kushner 2002), regional factors such as increase in black carbon concentrations in southern China (Menon et al. 2002), and troposphere–stratosphere exchange (Fueglistaler and Haynes 2005).

4. Change of large-scale circulation in climate models

Significant surface warming in the second half of the twentieth century in China, especially in northern China and in winter, has been reported in a number of studies (e.g., Karl et al. 1991; Wang and Gaffen 2001) and correlated with global warming. For Eurasia, the larger

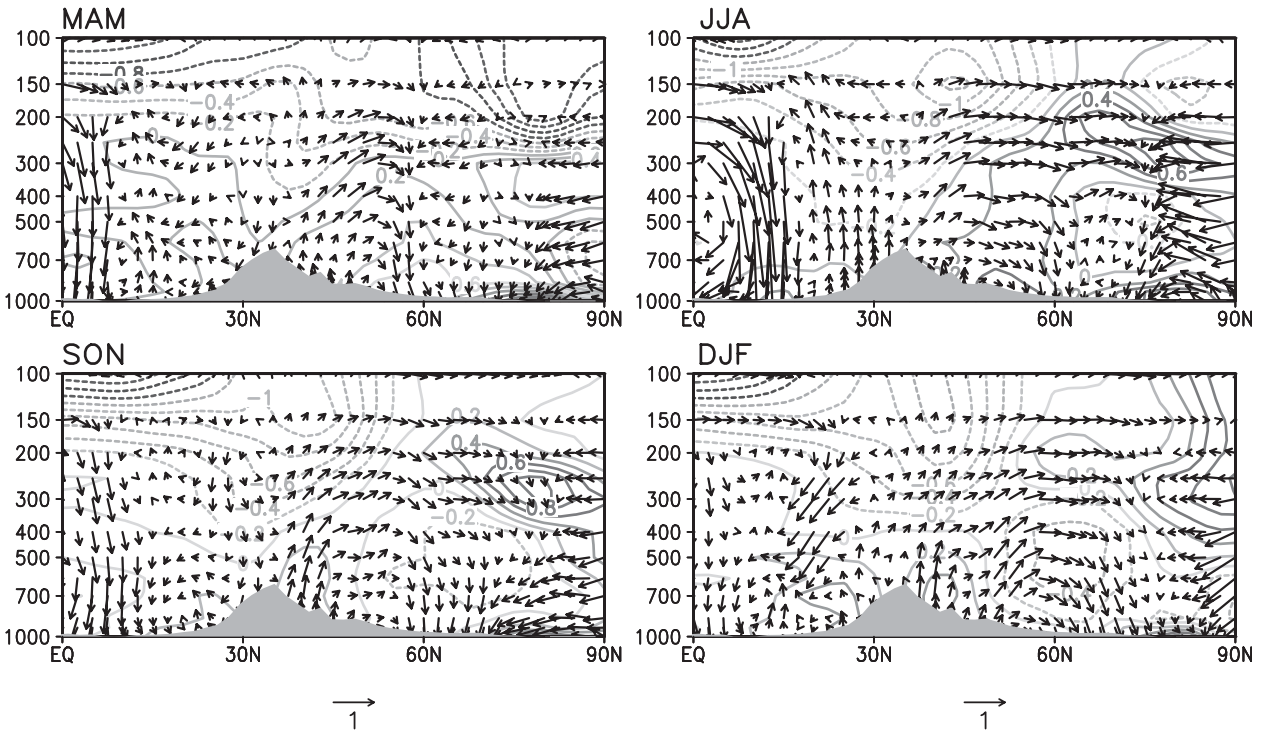

FIG. 8. Cross section of the LVRs in air temperature and meridional circulation averaged from 70° to 120°E during 1979–2003. The units of LVRs in temperature, meridional wind speed, and vertical velocity are °C decade^{-1}, m s^{-1} decade^{-1}, and Pa s^{-1} decade^{-1}, respectively. The vector is constructed from the LVRs as (v, $\omega \times -100$). Shaded areas denote topography.

land surface warming amplitude in the mid- and high latitudes than in the tropics has been listed as one of the most significant features of global change (Solomon et al. 2007). Zhou and Yu (2006) examined changes of the surface air temperature over China and the globe in the twentieth century simulated by 19 coupled climate models (including all 16 models in this study) driven by historical natural and anthropogenic forcings. Results indicate that most models except CSIRO Mk3.0 and FGOALS-g1.0 perform well in simulating both the global and the Northern Hemispheric mean surface air temperature evolution of the twentieth century. Unfortunately, present AOGCMs have serious defects in simulating regional climate. Kang et al. (2002) demonstrated that none of 10 models participating in the Climate Variability and Predictability (CLIVAR)/Monsoon GCM Intercomparison Project can realistically reproduce the observed mei-yu rain belt, and the situation is improved only slightly for the 16 AOGCMs participating in the second phase of the Coupled Model Intercomparison Project (CMIP2; Meehl et al. 2000). Hu et al. (2003) indicated that only three among these can reproduce the major features of the observed summer precipitation shift in China under the background of global warming. As introduced in section 2, the 16 AOGCMs investigated in this study come from CMIP3, with improved schemes for physical processes, increased spatial resolution, and the use of more natural and anthropogenic forcing factors.

The capability of AOGCMs to mimic the basic circulation pattern is a prerequisite to reproduce the past climate change and project the future climate trend. Since climate change is seasonally dependent and the most significant weakening trend in both SHF and the surface wind speed occurs in spring after the 1970s, here we focus on the changes in spring temperature and circulation of the numerical simulation results. In Fig. 9 we give the zonal wind speed at 500 hPa in MAM for each model. Although spatial resolution and schemes for physical process parameterization are different among those models, the basic features such as the location and intensity of the EASWJ generated agree well with the observations (top left panel in Fig. 4). The simulated strongest EASWJ occurs in IPSL CM4, in which the magnitude of wind speed usually exceeds 30 m s^{-1} in the North Pacific jet core.

The simulated 500-hPa air temperatures in all 16 AOGCMs under the 20C3M scenario do exhibit a clear trend over the Northern Hemisphere during 1979–2000, whereas a large spread exists in both amplitude and distribution among the 16 models (Fig. 10). Generally,

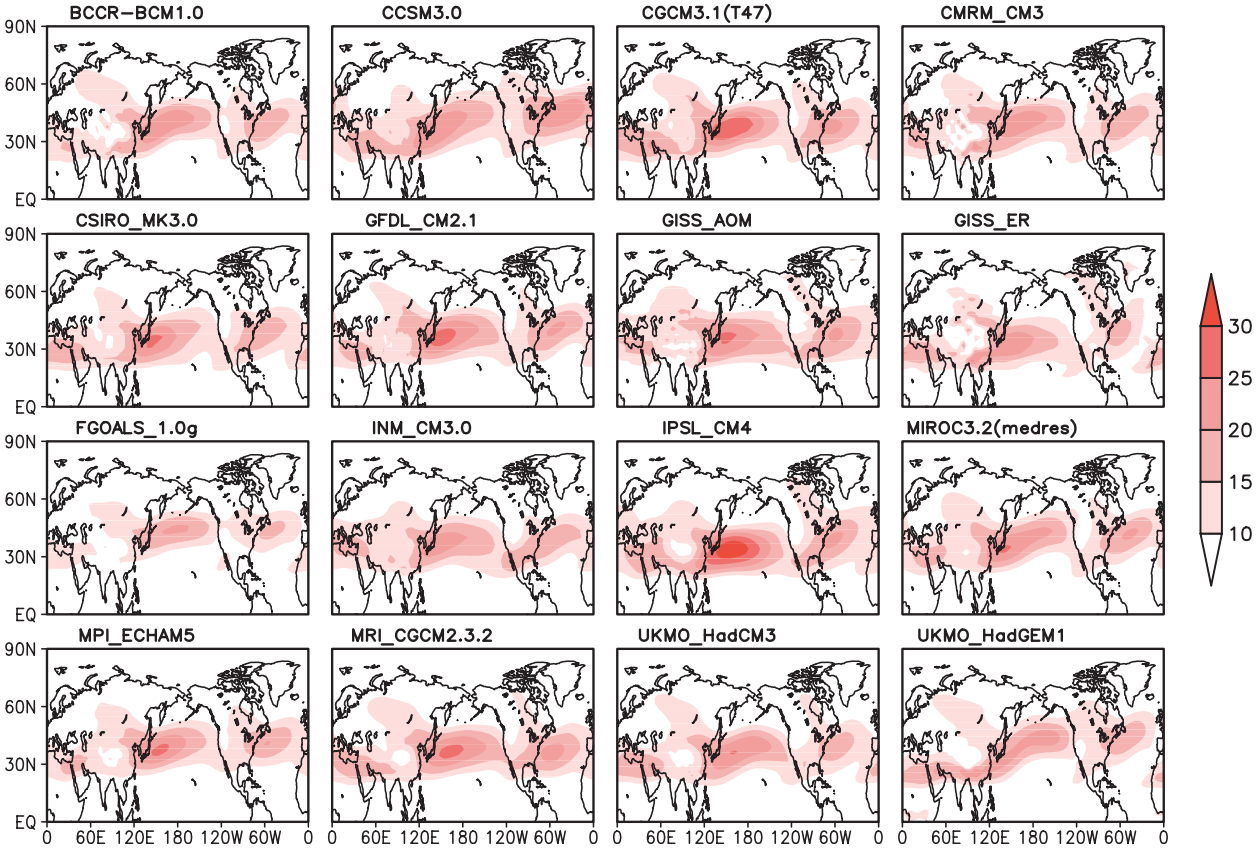

FIG. 9. MAM mean 500-hPa zonal wind speed in units of m s^{-1} during 1979–2000 for the 20C3M scenario in each model.

the simulated temperature trend in CSIRO Mk3.0, GISS-AOM, MIROC3.2(medres), and MPI ECHAM5 are similar to that in NCEP/DOE within the Eurasian domain, and all of them successfully reproduce the warming center around Baikal, with a comparable magnitude of about 0.6°C $decade^{-1}$. The feature of a larger warming trend in midlatitudes of Eurasia than in tropics is also reproduced in GISS-ER and UKMO HadGEM1, although the warming center moves somewhat to midlatitudes. However, in CNRM-CM3, INM-CM3.0, IPSL CM4, and UKMO HadCM3, the warming area in the mid- and high latitudes of Eurasia is replaced by a reversed cooling trend, accompanied by a subtropical warming belt covering from eastern China to the northern Pacific. Significant warming trend over the polar region is an important feature of the recent global warming, whereas a revised cooling trend occurs in CCSM3.0, CSIRO Mk3.0, FGOALS-g1.0, and MRI CGCM2.3.2. In fact, the large spread of the LVR in air temperature given by those models exists at all levels, with a similar spatial distribution from the surface to 300 hPa (figures not shown).

Consequently, the responses of the EASWJ to global warming, in terms of the 500-hPa EASWJ index in MAM during 1979–2000, are also variable among these models (Fig. 11). Considering the fact that the intensity of the climatological mean EASWJ varies among these models, to compare them conveniently, here we use the anomaly of the EASWJ index, with a reference period of 1979–2000. The corresponding LVR is also marked at the upper-right position in each panel. As indicated in Fig. 5, in NCEP/DOE, the LVR of the 500-hPa EASWJ index in MAM during 1979–2003 is -0.31 m s^{-1} $decade^{-1}$. Such a weakening trend in the simulated EASWJ index is significant in CSIRO Mk3.0, GISS-ER, MIROC3.2 (medres), MPI ECHAM5, and UKMO HadGEM1, with LVRs of -0.33, -0.22, -0.21, -0.37, and -0.52 m s^{-1} $decade^{-1}$, respectively. However, in CGCM3.1(T47), INM-CM3.0, IPSL CM4, and MRI CGCM2.3.2, we see a significant intensifying trend in the EASWJ, and there is no significant change in the rest of the models.

Table 1 shows that there is no direct relationship between the model resolution and the capability of reproducing the change in the EASWJ. Notice that the common forcing fields of greenhouse gases and sulfate aerosol direct effects have been imposed in all models, whereas the other influences such as sulfate aerosol indirect effects and tropospheric and stratospheric ozone

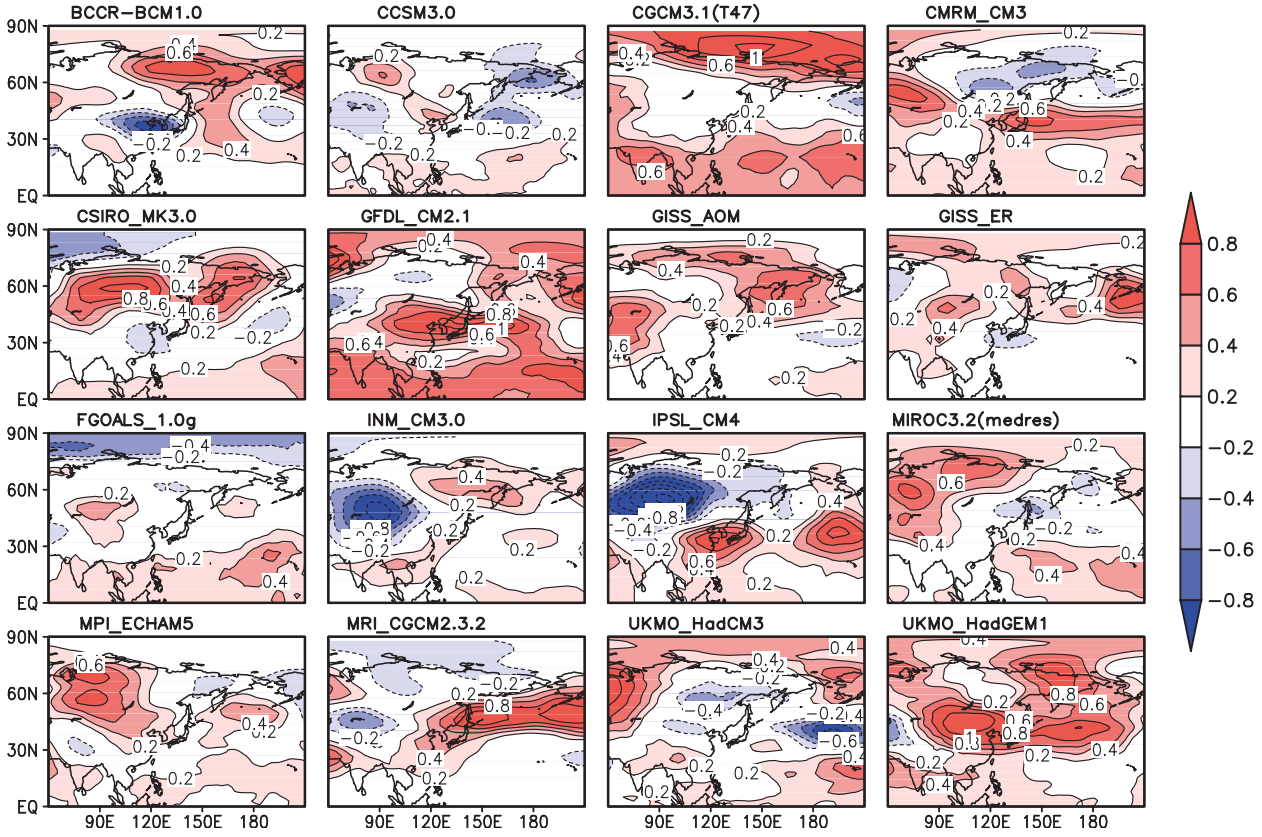

FIG. 10. Spatial distribution of the simulated LVR for MAM air temperature (°C decade^{-1}) at 500 hPa during 1979–2000.

are simultaneously included only in 5 of 6 models that have successfully reproduced the weakening trend in EASWJ. This implies the importance of the latter in influencing the temperature trend. Indeed, the role of sulfate aerosol indirect effects in influencing EASM activity and climate change during the last half of the twentieth century in EA has been emphasized separately by Qian and Giorgi (1999), Xu (2001), and Lau et al. (2008). On the other hand, ozone depletion in EA has been demonstrated as having a direct connection with the recent local temperature change in the upper atmosphere through both data analysis and numerical modeling (Zhou and Zhang 2005; Duan 2007). The relative importance of all these natural and anthropogenic forcings and the physics governing these responses need further investigation in the future. Cloud–radiation feedback in AOGCMs and atmospheric teleconnections may also have contributions. However, this is beyond the scope of this study.

On the time sale of interannual variability, the difference between models and NCEP/DOE is remarkable. For example, in NCEP/DOE, the weakest EASWJ happens in 1981 and 1997, but none of these models can reproduce both of them. It suggests that there is still room to improve the current state-of-art coupled climate models so as to capture the atmospheric variability in all time scales.

As discussed before, in the free atmosphere, meridional geostrophic balance determines the seasonal mean zonal wind in both sign and strength. Hence the change in the EASWJ must be accompanied by a reduction of the meridional temperature and pressure gradients along the jet axis. This point is further verified in Fig. 12, in which the temperature difference between two boxes (35°–55°N, 120°E–0° and 15°–35°N, 70°–120°E) is defined as the EASWJ related meridional temperature gradient. Obviously, the temperature gradient is proportional to the strength of the EASWJ, and a coherent trend between them can be seen in all 16 models. Note that the meridional temperature gradient is negative, and a positive LVR means a reduction of it.

5. Summary and discussion

In Part I we have shown an obvious weakening trend in the heating source over the TP during 1980–2003. SHF acts as a dominant component of the total heating source in spring, and its weakening trend is induced mainly by declined surface wind speed. Using historical

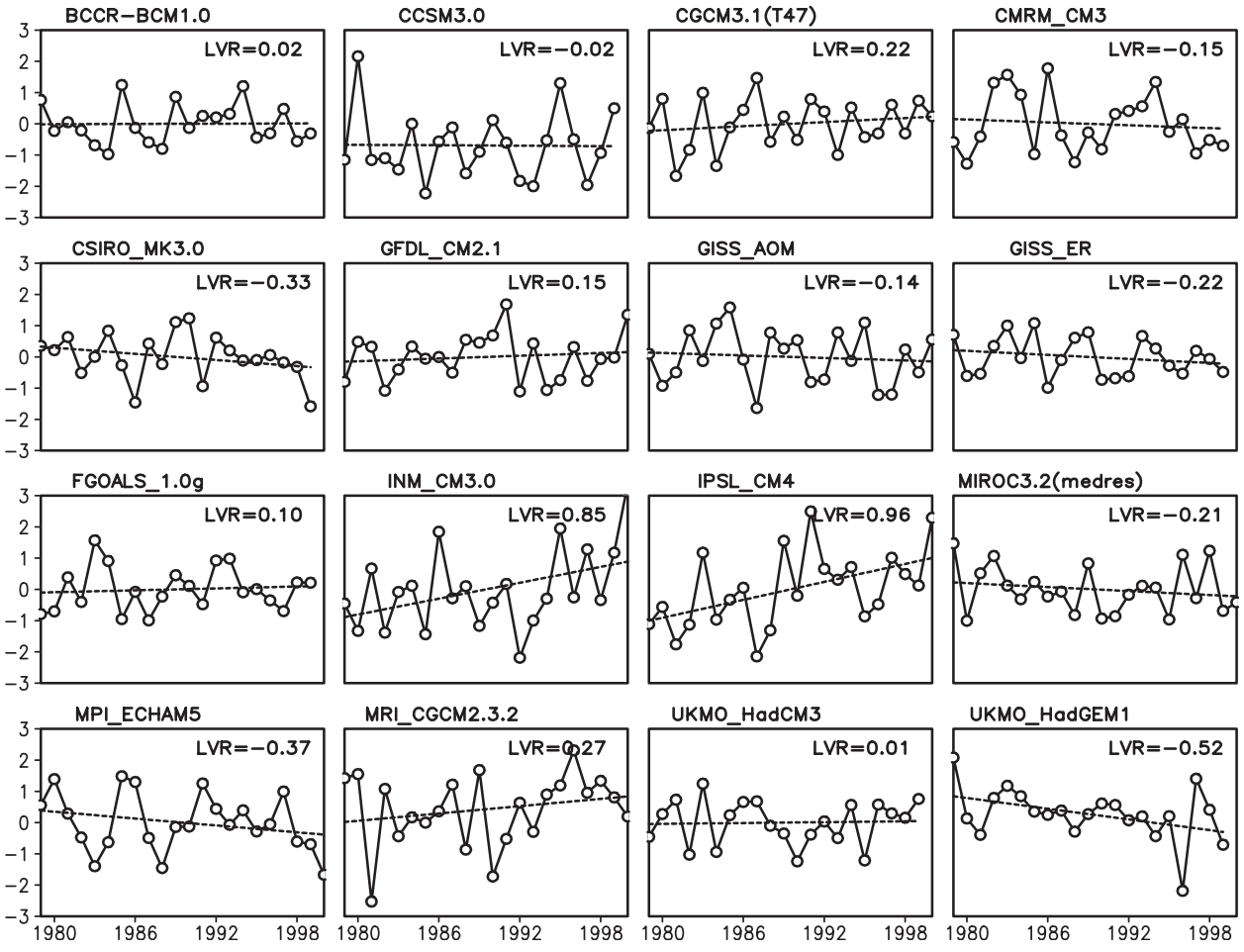

FIG. 11. Simulated temporal evolution (solid curves) and LVR (dashed lines) of the 500-hPa EASWJ index in MAM during 1979–2000. Units for the EASWJ and its LVR are m s^{-1} and m s^{-1} $decade^{-1}$, respectively.

records and NCEP/DOE reanalysis, the mechanism of such a change, and in particular its relationship with the large-scale circulation shift under the background of the twentieth-century global warming, is further investigated in this paper. In addition, a multimodel intercomparison is carried out to verify the diagnosis results. The major conclusions are summarized as follows:

- During the period of 1979–2003, substantial warming in the mid- and high latitudes over eastern Eurasia leads to decreased meridional temperature and pressure gradients over the subtropics to the south. As a consequence of the geostrophic balance relationship, the EASWJ presents a significant decreasing trend throughout most parts of the year. Since the near-surface winds over the TP depend mainly on the midtropospheric EASWJ, which straddles the TP in all seasons except in summer, the declined wind speed and the suppressed spring heating source over the TP are closely related to the decreasing trend in EASWJ.
- Meanwhile, the local Ferrel cell over EA shows a coherent weakening trend, with anomalous descending motion by 60°N but anomalous ascending motion around 40°N. The change of the spring local Hadley cell almost shows an opposite signal to its climate mean, represented by a clear weakening trend in its equatorial ascending branch.
- Not all of the 16 climate models can successfully reproduce the observed change in air temperature and the EASWJ when driven by historical natural and anthropogenic forcings during the twentieth century. Intercomparison results among these modes suggest that sulfate aerosol indirect effects and ozone may be important in reproducing the weakening trend in EASWJ. The performance of these models under the 20C3M scenario seems have no direct relationship with the model resolution. Instead, whether they are able to reproduce the observed spatial distribution of the large-scale air temperature change is vital in simulating the observed trend in the EASWJ.

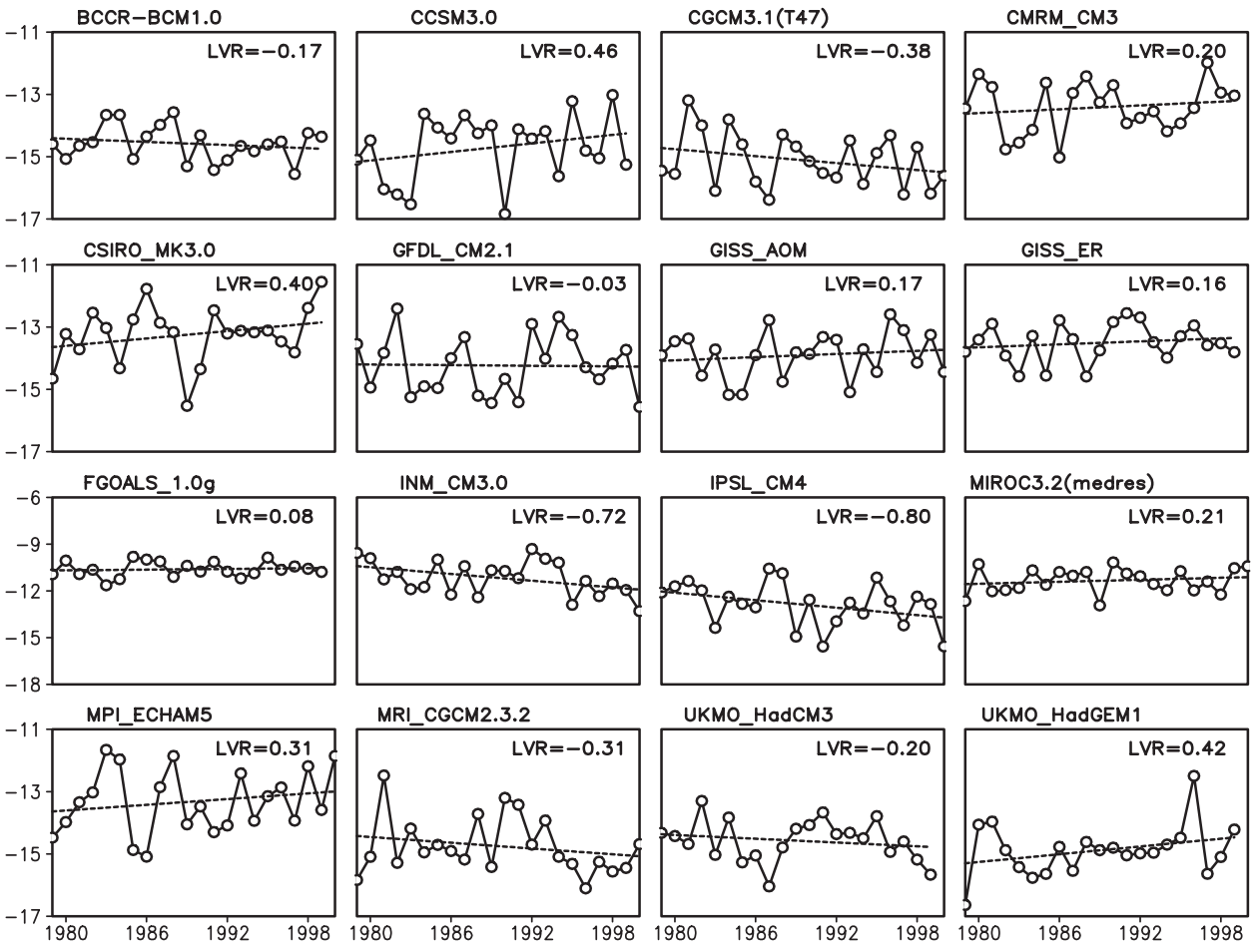

FIG. 12. Simulated temporal evolution of 500-hPa meridional temperature gradient along 35°N (solid curves) represented by (35°–55°N, 70°–120°E) minus (15°–35°N, 70°–120°E) and its LVR (dashed lines) during 1979–2000. Units of temperature and LVR are °C and °C decade^{-1}, respectively.

When driven by historical natural and anthropogenic forcings, most of the current state-of-the-art coupled climate models perform acceptably in simulating the major variations of the surface air temperature averaged over China, whereas there are large deficiencies in simulating the spatial distributions (Zhou and Yu 2006). Here, we show that this is also true in the upper layers. To understand what causes the spread among different climate models is not only critical for recognizing the role of climate variability, but it is also beneficial to improvement of the climate models. In this regard, it is desirable to further evaluate the relative importance of the parameterization schemes for physical processes such as cloud–radiation feedback and convective activity.

Hori and Ueda (2006) investigated the impacts of global warming on the EA winter monsoon in the future by using 9 AOGCMS (8 of them are employed in this study). Their results suggest that, under a global warming scenario, most models show a weakening trend in the EA winter monsoon, accompanied by a strong anticyclonic anomaly over the North Pacific corresponding to a weakened and/or northern shifted Aleutian low. As a result, the pressure gradient along the eastern coast of the Eurasian continent, the local Hadley circulation, and the EASWJ will be reduced. As discussed in section 3, all these phenomena have already happened during recent decades, and the simulation results in this study resemble those in Hori and Ueda (2006), although some details are different.

Climate variations are well known for their complexity due to the impacts of many factors over a wide range of spatial and temporal scales. Yu and Zhou (2007) argue that the general atmospheric circulation over EA is characterized by vivid seasonality and a three-dimensional structure. Besides the depressed EASM activity after the end of the 1970s, climate change in other aspects in EA—such as the enhancement and southwestward extension of the western Pacific subtropical high (Nitta

and Hu 1996; Hu 1997), the cooling trend in the upper troposphere and lower stratosphere, and the warming trend in the mid- and lower troposphere—have also been documented (Duan 2007). Other factors, for example, the SST of global oceans, snow cover and soil moisture in Eurasia, and the natural variability of the climate system, may also contribute to these changes to a certain degree.

As discussed in Part I, the enhanced radiative cooling of air column is listed along with other factors for the weakening trend in the atmospheric heating source over the TP. This might be related to the decreased in situ total cloud amount (Duan and Wu 2006), because the plateau climate is characterized by intense radiative cooling, solar radiative heating, and more important modulating effects on the local cloud amount. Therefore, compared to the large-scale circulation shift induced by global warming, the enhanced radiative cooling effect over the TP may be associated more directly with local climate change. A detailed physical interpretation is then required.

Moreover, the response of the EASM to such a trend in the heating source over the TP still remains unknown. Numerical simulation studies will be carried out in our future work to answer this question.

Acknowledgments. The authors are very grateful to three anonymous reviewers for their helpful and constructive comments and suggestions in modifying the manuscript. We acknowledge the CMIP international modeling groups for providing their data for analysis, PCMDI for collecting and archiving the model data, the JSC/CLIVAR WGCM and their CMIP and Climate Simulation Panel for organizing the model data analysis activity, and the IPCC WG1 TSU for technical support. The IPCC Data Archive at Lawrence Livermore National Laboratory is supported by the Office of Science, U.S. Department of Energy. The authors thank Drs. Tianjun Zhou and Jiandong Li for providing the archived CMP3 modeling results. This work was jointly supported by the Chinese Ministry of Science and Technology under Grants 2006CB403607 and 2009CB421403, the Chinese Academy of Sciences under Grant KZCX2-YW-Q11-01, the Innovation Key Program (Grant KZCX2-YW-BR-14) of the Chinese Academy of Sciences under the Grants KZCX2-YW-BR-14, ''Hundred Talent Program'' of the Chinese Academy of Sciences, and the Chinese National Science Foundation under Grants 40875034 and 40821092.

REFERENCES

Ding, Y., and Y. Sun, 2004: Changes in Asian summer monsoon and possible mechanisms. *Climate Change Newsletter 2003/2004,* China IPCC Office, 47–49

Duan, A. M., 2007: Cooling trend in the upper troposphere and lower stratosphere over China. *Geophys. Res. Lett.,* **34,** L15708, doi:10.1029/2007GL029667.

——, and G. Wu, 2006: Change of cloud amount and the climate warming on the Tibetan Plateau. *Geophys. Res. Lett.,* **33,** L22704, doi:10.1029/2006GL027946.

——, and ——, 2008: Weakening trend in the atmospheric heat source over the Tibetan Plateau during recent decades. Part I: Observations. *J. Climate,* **21,** 3149–3164.

——, Y. M. Liu, and G. X. Wu, 2005: Heating status of the Tibetan Plateau from April to June and rainfall and atmospheric circulation anomaly over East Asia in midsummer. *Sci. China,* **48D,** 250–257, doi:10.1360/02yd0510.

——, G. X. Wu, Q. Zhang, and Y. M. Liu, 2006: New proofs of the recent climate warming over the Tibetan Plateau as a result of the increasing greenhouse gases emissions. *Chin. Sci. Bull.,* **51,** 1396–1400.

Flohn, H., 1957: Large-scale aspects of the summer monsoon in South and East Asia. *J. Meteor. Soc. Japan,* **35,** 180–186.

Fueglistaler, S., and P. H. Haynes, 2005: Control of interannual and longer-term variability of stratospheric water vapor. *J. Geophys. Res.,* **110,** D24108, doi:10.1029/2005JD006019.

Gong, D. Y., and C. H. Hu, 2002: Shift in the summer rainfall over the Yangtze River valley in the late 1970s. *Geophys. Res. Lett.,* **29,** 1436, doi:10.1029/2001GL014523.

Hahn, D. G., and S. Manabe, 1975: The role of mountains in the south Asian monsoon circulation. *J. Atmos. Sci.,* **32,** 1515–1541.

Holton, J. R., 1992: *An Introduction to Dynamic Meteorology*. Academic Press, 511 pp.

Hori, M. E., and H. Ueda, 2006: Impact of global warming on the East Asian winter monsoon as revealed by nine coupled atmosphere-ocean GCMs. *Geophys. Res. Lett.,* **33,** L03713, doi:10.1029/2005GL024961.

Hu, Y., and Q. Fu, 2007: Observed poleward expansion of the Hadley circulation since 1979. *Atmos. Chem. Phys.,* **7,** 5229–5236.

——, K. K. Tung, and J. Liu, 2005: A closer comparison of early and late winter atmospheric trends in the Northern Hemisphere. *J. Climate,* **18,** 2924–2936.

Hu, Z. Z., 1997: Interdecadal variability of summer climate over East Asia and its association with 500 hPa height and global sea surface temperature. *J. Geophys. Res.,* **102,** 19 403–19 412.

——, S. Yang, and R. Wu, 2003: Long-term climate variations in China and global warming signals. *J. Geophys. Res.,* **108,** 4614, doi:10.1029/2003JD003651.

Kalnay, E., and Coauthors, 1996: The NCEP/NCAR 40-Year Reanalysis Project. *Bull. Amer. Meteor. Soc.,* **77,** 437–471.

Kanamitsu, M., W. Ebisuzaki, J. Woollen, S.-K. Yang, J. J. Hnilo, M. Fiorino, and G. L. Potter, 2002: NCEP–DOE AMIP-II Reanalysis (R-2). *Bull. Amer. Meteor. Soc.,* **83,** 1631–1643.

Kang, I. S., and Coauthors, 2002: Intercomparison of the climatological variations of Asian summer monsoon precipitation simulated by 10 GCMs. *Climate Dyn.,* **19,** 383–395.

Karl, T. R., G. Kukla, V. Razuvaev, M. Changery, R. Quayle, R. Heim Jr., D. Easterling, and C. Fu, 1991: Global warming: Evidence for asymmetric diurnal temperature change. *Geophys. Res. Lett.,* **18,** 2253–2256.

Lau, K.-M., and Coauthors, 2008: The joint aerosol–monsoon experiment: A new challenge for monsoon climate research. *Bull. Amer. Meteor. Soc.,* **89,** 369–383.

Lu, J., G. A. Vecchi, and T. Reichler, 2007: Expansion of the Hadley cell under global warming. *Geophys. Res. Lett.,* **34,** L06805, doi:10.1029/2006GL028443.

Meehl, G. A., G. J. Boer, C. Covey, M. Latif, and R. J. Stouffer, 2000: The Coupled Model Intercomparison Project (CMIP). *Bull. Amer. Meteor. Soc.,* **81,** 313–318.

Menon, S., J. Hansen, L. Nazarenko, and Y. Luo, 2002: Climate effects of black carbon aerosols in China and India. *Science,* **297,** 2250–2253.

Nitta, T., and S. Yamada, 1989: Recent warming of tropical sea surface temperature and its relationship to the Northern Hemisphere circulation. *J. Meteor. Soc. Japan,* **67,** 375–383.

——, and Z. Z. Hu, 1996: Summer climate variability in China and its association with 500 hPa height and tropical convection. *J. Meteor. Soc. Japan,* **74,** 425–445.

Polvani, L. M., and P. J. Kushner, 2002: Tropospheric response to stratospheric perturbations in a relatively simple general circulation model. *Geophys. Res. Lett.,* **29,** 1114, doi:10.1029/2001GL014284.

Qian, Y., and F. Giorgi, 1999: Interactive coupling of regional climate and sulfate aerosol models over eastern Asia. *J. Geophys. Res.,* **104,** 6477–6499.

Solomon, S., D. Qin, M. Manning, M. Marquis, K. Averyt, M. M. B. Tignor, H. L. Miller Jr., and Z. Chen, Eds., 2007: *Climate Change 2007: The Physical Science Basis*. Cambridge University Press, 996 pp.

Tao, S. Y., and L. X. Chen, 1987: A review of recent research on the East Asian summer monsoon in China. *Monsoon Meteorology,* C. P. Chang and T. N. Krishnamurti, Eds., Oxford University Press, 60–92.

Trenberth, K. E., and J. W. Hurrell, 1994: Interdecadal atmosphere-ocean variations in the Pacific. *Climate Dyn.,* **9,** 303–319.

Uppala, S. M., and Coauthors, 2005: The ERA-40 Re-Analysis. *Quart. J. Roy. Meteor. Soc.,* **131,** 2961–3012.

Wang, J. X. L., and D. J. Gaffen, 2001: Late-twentieth-century climatology and trends of surface humidity and temperature in China. *J. Climate,* **14,** 2833–2845.

Xu, M., C.-P. Chang, C. Fu, Y. Qi, A. Robock, D. Robinson, and H. Zhang, 2006: Steady decline of East Asian monsoon winds, 1969-2000: Evidence from direct ground measurements of wind speed. *J. Geophys. Res.,* **111,** D24111, doi:10.1029/2006JD007337.

Xu, Q., 2001: Abrupt change of the mid-summer climate in central east China by the influence of atmospheric pollution. *Atmos. Environ.,* **35,** 5029–5040.

Yanai, M., C. Li, and Z. Song, 1992: Seasonal heating of the Tibetan Plateau and its effects on the evolution of the Asian summer monsoon. *J. Meteor. Soc. Japan,* **70,** 319–351.

Yeh, D. Z., and B. Z. Zhu, 1955: The onset of the transitional seasons in the Far East from the viewpoint of the general circulation (in Chinese). *Acta Meteor. Sin.,* **26,** 71–87.

——, and Y. X. Gao, 1979: *Meteorology of the Qinghai-Xizang (Tibet) Plateau*. Science Press, 278 pp.

Yin, M. T., 1949: A synoptic-aerological study of the onset of the summer monsoon over India and Burma. *J. Meteor.,* **6,** 393–400.

Yu, R., and T. Zhou, 2007: Seasonality and three-dimensional structure of interdecadal change in the East Asian monsoon. *J. Climate,* **20,** 5344–5355.

——, B. Wang, and T. J. Zhou, 2004: Tropospheric cooling and summer monsoon weakening trend over East Asia. *Geophys. Res. Lett.,* **31,** L22212, doi:10.1029/2004GL021270.

Zhang, Y. C., X. Y. Kuang, W. D. Guo, and T. J. Zhou, 2006: Seasonal evolution of the upper-tropospheric westerly jet core over East Asia. *Geophys. Res. Lett.,* **33,** L11708, doi:10.1029/2006GL026377.

Zhao, P., and L. X. Chen, 2001: Climate features of atmospheric heat source/sink over the Qinghai-Xizang Plateau in 35 years and its relation to rainfall in China. *Sci. China,* **44D,** 858–864.

Zhou, S. W., and R. H. Zhang, 2005: Decadal variations of temperature and geopotential height over the Tibetan Plateau and their relations with Tibet ozone depletion. *Geophys. Res. Lett.,* **32,** L18705, doi:10.1029/2005GL023496.

Zhou, T. J., and R. C. Yu, 2006: Twentieth-century surface air temperature over China and the globe simulated by coupled climate models. *J. Climate,* **19,** 5843–5858.